Original Article

Institution of MECHANICAL ENGINEERS

Journal of MULTI-BODY DYNAMICS

Proc IMechE Part K:
J Multi-body Dynamics
2019, Vol. 233(1) 174–181

DOI: 10.1177/1464419318793503
journals.sagepub.com/home/pik

SAGE

Modeling and control of a flapping wing robot

Abdolbaghi Bakhtiari, Shahram Ehtemadi Haghighi and Adel Maghsoudpour

Abstract

The dynamics and control of a flapping wing robot are studied in this paper which helps to develop a complete dynamic model for the robot consisting of tail effects and also enhance the path tracking control of the robot. In the first part of the paper, the aerodynamic model of the wings is presented, and an aerodynamic force model for the tail is introduced which includes the leading edge suction effects. An experiment is also carried out on a flapping wing robot in a laboratory environment to evaluate the forces on the tail and its result will be compared with the results of the model presented for the tail. In the second part, a controller is designed for the robot. This controller uses the nonlinear dynamic inversion method to solve the nonlinear equations of the control system. The experimental results of the tail forces agree well with the theoretical predictions and reveal that the tail aerodynamics are affected by leading edge suction. Also, simulation results show that the competence performance and convergence performance of the designed controller are obtained.

Keywords

Flapping wing robot, nonlinear control, path tracking

Date received: 15 February 2018; accepted: 3 July 2018

Introduction

During recent decades, considerable theoretical studies on flapping plates have been conducted. The flapping plate can be used to model the wing of flying animals[1,2,3] and also to model airplane wing flutter or helicopter swash plate dynamics.[4,5] The purpose of the present study is to model and control a flapping wing robot. Flapping wings create complicated movements that are more complex than fixed wings and this make flapping wing robots difficult to model.

Despite their complexity, dynamic modeling of flapping wings has been studied by many researchers. One of the first models to calculate the forces acting on a flapping wing, based on a potential flow approach, was presented by Jones.[1] Ellington[2] provided a comprehensive model for kinematics of a small-scale flapping wing that includes coupling of wing rotation with translation. Delaurier[3] also provided a useful model based on a modified strip theory for calculating the unsteady aerodynamic forces generated by flapping wings. The model also represents an expression for stall angle in flapping wings. Other researchers developed the Delaurier model for the analysis of various wing shapes with phase lag between flapping and pitching motion in them.[6–8] Shyy et al.[9] also studied the aerodynamics of flapping wing micro air vehicles (MAVs) with special focus on small MAVs and membrane wings. The tail also has a significant effect on the dynamics and control of the flapping wing robot in addition to that of the wings.[10] However, little studies about modeling the tail and its use in controlling the robot have been done.[11] The control system is necessary to ensure the stability and performance of the autonomous ornithopter and many research works have been performed in this regard. One of the first control schemes that proposed hovering kinematics for flapping wings was presented by Schenato et al.[12] Deng et al.[13] also have studied system modeling and control design of flapping wing vehicles. They modeled lift and drag on the wing using standard quasi-steady aerodynamics and also formulated a high-frequency periodic control problem for the flapping wing vehicles. Most of the

Department of Mechanical and Aerospace Engineering, Science and Research Branch, Islamic Azad University, Tehran, Iran

Corresponding author:
Shahram Etemadi Haghighi, Department of Mechanical and Aerospace Engineering, Science and Research Branch, Islamic Azad University, Tehran, Iran.
Email: setemadi@srbiau.ac.ir

control systems designed for the flapping wing robots used wing frequency of flapping and mean angle of attack as control variables to adjust the center of gravity of the robot[14–16] but as will be discussed in the following list, the tail has considerable effect on dynamics of the flapping wing robot and can be used as a control parameter.

Comparing with existing works, the main contributions of present work lie in two aspects:

1. A complete dynamic model for flapping wings and tail of the robot is presented. The tail aerodynamics is modeled using the leading-edge-suction analogy which covers high angles of attack and completes the previous studies that only considered low angle of attacks (AOAs).[9] Also, the results obtained from the analytical model are compared with the results of a wind tunnel test performed in the present study.
2. After developing the dynamic model of the robot which is highly nonlinear, a controller is designed based on nonlinear dynamic inversion (NDI) approach. The designed control system uses tail in addition to the wings to control the robot. Also, the performance of the control system is tested by guiding the robot to track a circular path.

This paper can be outlined as follows. In section "Dynamic modeling of the flapping wing robot," the model developed by Delaurier is used to calculate the forces acting on the wings. Section "Tail aerodynamic" presents the model developed for calculating the aerodynamic forces exerted on the tail and also compare the model with experimental results. The controller design is stated in section "Control design" and simulation results of controlling the robot are demonstrated in section "Simulation results" followed by a brief conclusion in the final section.

Dynamic modeling of the flapping wing robot

Dynamics of robot motions

This section presents the dynamic model of the flapping wing robot. The wings and the tail apply forces to body and giving it the ability for flight. Figure 1 shows the inertial and body frames of the robot.

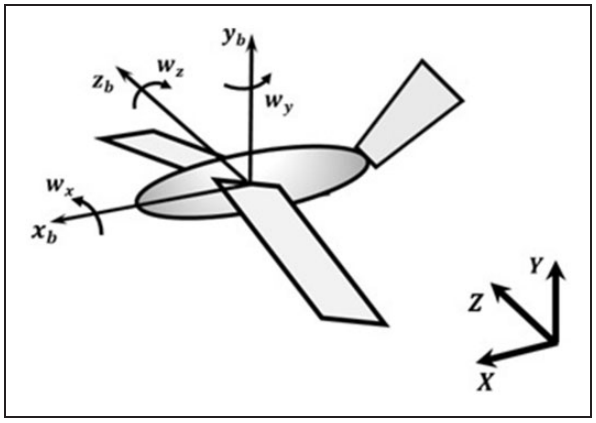

Figure 1. Coordinate systems of the robot.

The general equations governing the robot can be written as follows

$$\begin{bmatrix} mI & 0 \\ 0 & I \end{bmatrix}\begin{bmatrix} \dot{v}^b \\ \dot{w}^b \end{bmatrix} + \begin{bmatrix} \omega^b \times mv^b \\ w^b \times Iw^b \end{bmatrix} = \begin{bmatrix} f^b \\ \tau^b \end{bmatrix} \tag{1}$$

In the above-mentioned equation, the b superscripts represent the body coordinate. Having the general force and torques exerted on the robot, the linear and angular velocities can be calculated in the body coordinates. The following equation shows the relationship between velocities in body and inertial frames.

$$\begin{bmatrix} \dot{X} \\ \dot{Y} \\ \dot{Z} \end{bmatrix} = \begin{bmatrix} cos\theta_y cos\theta_z & -sin\theta_y cos\theta_x + cos\theta_y sin\theta_z sin\theta_x & sin\theta_y sin\theta_x + cos\theta_y sin\theta_z cos\theta_x \\ sin\theta_y cos\theta_z & cos\theta_y cos\theta_x + sin\theta_y sin\theta_z sin\theta_x & -cos\theta_y sin\theta_x + sin\theta_y sin\theta_z cos\theta_x \\ -sin\theta_z & cos\theta_z sin\theta_x & cos\theta_z cos\theta_x \end{bmatrix}.v^b \tag{2}$$

The relationship between velocity vector $\begin{bmatrix} \dot{\theta}_x & \dot{\theta}_y & \dot{\theta}_z \end{bmatrix}^T$ and the vector ω^b is also as follows

$$\begin{bmatrix} \dot{\theta}_x \\ \dot{\theta}_y \\ \dot{\theta}_z \end{bmatrix} = \begin{bmatrix} 0 & \frac{sin\theta_x}{cos\theta_z} & \frac{cos\theta_x}{cos\theta_z} \\ 0 & cos\theta_x & -sin\theta_x \\ 1 & sin\theta_x tan\theta_z & cos\theta_x tan\theta_z \end{bmatrix}.\omega^b \tag{3}$$

The forces exerted on the robot body are shown in Figure 2.

The aerodynamic forces are obtained by flapping wings, and any change in flapping mechanism will change the aerodynamic forces too. The following assumptions will be applied on equation (1) for simplicity:

1. The forces exerted on the wings are assumed as the average of generated force during a flapping cycle.
2. The center of mass of the robot is assumed to be on the line that connecting the center of the wings,

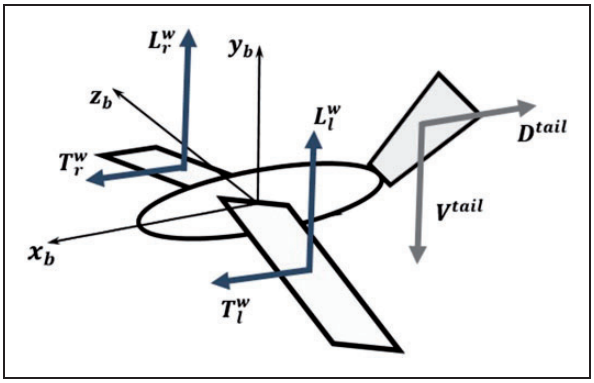

Figure 2. Aerodynamic forces exerted on robot.

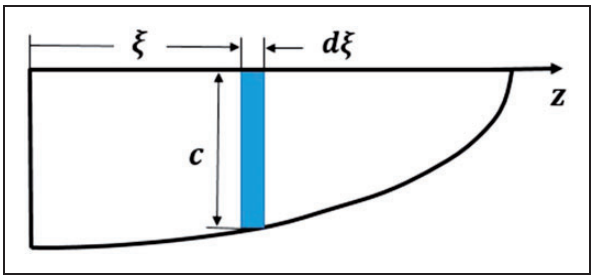

Figure 3. Strips on the wing.

and so the force of the wings has no moment about z_b axis.

3. The wings have similar flapping angles and the total moment caused by them about x_b-axis is zero.

Wing aerodynamics

In the present study, the model developed by Delaurier is used to calculate the forces exerted on the wings. In this model, the wing is divided into parallel strips and the force applied to each stripe is calculated according to its position and velocity as shown in Figure 3.

The total forces exerted on the wing are also obtained from the sum of the force applied to all $d\xi$ strips. These forces depend on the wings angles of attack and flapping at any time. These two angles are shown in Figure 4.

β in Figure 4 is the angle of the flapping, which also changes as a sinusoidal function with time during flapping

$$\beta = \beta_0 sin(2\pi vt) \tag{4}$$

φ is also the wing's angle of attack relative to U_∞ direction. This angle varies along the wing and is obtained from the sum of three angles:

1. φ_w is the angle of wing section with flapping axis (x_b axis) that is connected to the robot body. This angle is defined in equation (5).

$$\varphi_w = \varphi_{w0} cos(2\pi vt) \tag{5}$$

2. The angle φ_b is the angle of flapping axis with respect to U_∞ and depends only on the orientation of the robot.
3. The angle $\delta\varphi$ is the change in the angle of attack along the wing due to its flexibility and its value can be defined in equation (6).

$$\delta\varphi = \xi^n \cos(2\pi vt) \tag{6}$$

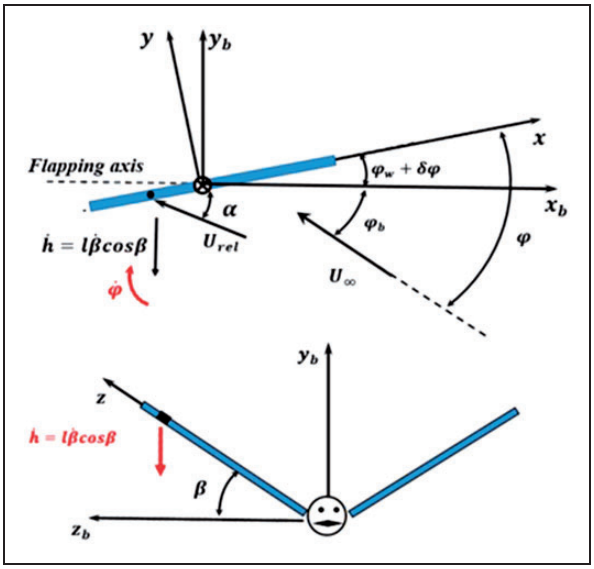

Figure 4. Flapping and pitching angles of the wing.

According to equation (6), the value of $\delta\varphi$ depends on ξ and n is a function of the wing's flexibility.

According to Figure 4, the sum of velocities $\dot{h}$ and U_∞ forms the relative velocity U_{rel}, which is used to calculate the aerodynamic forces acting on the wing. The vector U_{rel} and its angle can be expressed by

$$U_{rel} = \left\{ \left[U_\infty sin\varphi + l\dot{\beta} cos\beta cos(\varphi_w + \delta\varphi) \right]^2 + \left[U_\infty cos\varphi - l\dot{\beta} cos\beta sin(\varphi_w + \delta\varphi) \right]^2 \right\}^{\frac{1}{2}}$$

$$\alpha = tan^{-1}\left[\frac{U_\infty sin\varphi + l\dot{\beta} cos\beta sin(\varphi_w + \delta\varphi)}{U_\infty cos\varphi - l\dot{\beta} cos\beta sin(\varphi_w + \delta\varphi)} \right] \tag{7}$$

The aerodynamic force exerted on the wing can be calculated in a variety of ways.[6,17,18] This forces are shown in Figure 5.

The forces dN, dD, and dT_S, which correspond to normal, drag, and thrust force, respectively, can be calculated as follows[8]

$$dN = \frac{\rho UV}{2} 2\pi(\alpha + \varphi) c d\xi$$

$$dD = C_D \rho \frac{V_x^2}{2} c d\xi$$

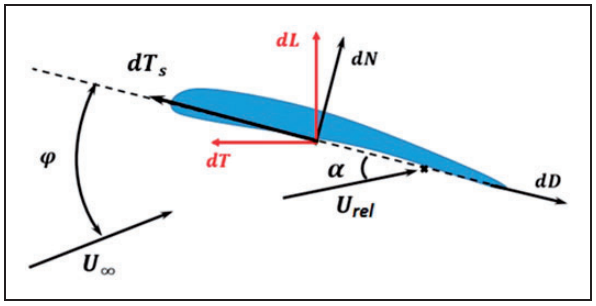

Figure 5. Wing section aerodynamic forces.

$$dT_S = \frac{\rho UV}{2} 2\pi \left(\alpha + \varphi - \frac{1}{4}\frac{c\dot{\varphi}}{U}\right)^2 cd\xi \tag{8}$$

The forces dL and dT can be obtained by the following equation[8]

$$\begin{aligned} dL &= dN cos\varphi + (mdT_S - dD) sin\varphi \\ dT &= (dT_S - dD) cos\varphi - dN sin\varphi \end{aligned} \tag{9}$$

The total forces exerted on the wing, as shown in Figure 2, can be expressed as follows

$$\begin{aligned} L^w &= \int_0^l dL = \int_0^l \left(\left(\frac{\rho UV}{2} 2\pi(\alpha + \varphi) \right) \cos\varphi \right. \\ &\quad \left. + \left(\frac{\rho UV}{2} 2\pi \left(\alpha + \varphi - \frac{1}{4}\frac{c\dot{\varphi}}{U} \right)^2 - C_D \rho \frac{V_x^2}{2} \right) sin\varphi \right) cd\xi \\ T^w &= \int_0^l dT = \int_0^l \left(\left(\frac{\rho UV}{2} 2\pi \left(\alpha + \varphi - \frac{1}{4}\frac{c\dot{\varphi}}{U} \right)^2 \right. \right. \\ &\quad \left. \left. - C_D \rho \frac{V_x^2}{2} \right) cos\varphi + \left(\frac{\rho UV}{2} 2\pi(\alpha + \varphi) \right) sin\varphi \right) cd\xi \end{aligned} \tag{10}$$

Tail aerodynamic

In this section, a model for the aerodynamic force on the tail is presented and the results from it are compared with the test results. Figure 6 shows the tail and its angles with respect to body of the robot.

In Figure 6, ψ and γ are the Roll and pitch angles of the tail, respectively. These two angles are used as tail control inputs. The tail's aerodynamics depends entirely on its pitch angle γ, at low γ, the flow around the tail is laminar, and the forces exerted on it can be calculated by calculating pressure difference between the upper and lower surfaces of the tail.[19] As γ increases, the leading edge vortices form around tail edges, as shown in Figure 7.

In this case, the leading edge vortices produce an additional force on the tail.[20] In the present study, due to the similarity of the tail of the robot with the delta wings, the aerodynamic model obtained for this type

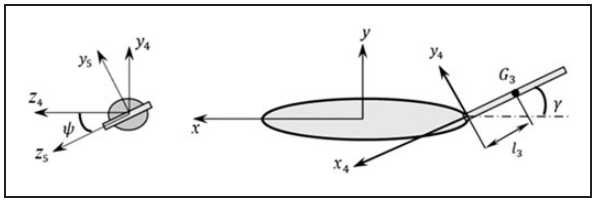

Figure 6. Tail degrees of freedom.

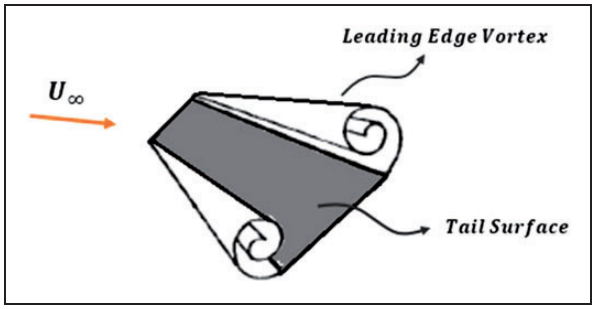

Figure 7. Leading edge vortex around tail.

of wings is also used for the tail. The forces imposing on a delta wing are presented below

$$\begin{aligned} V^{tail} &= \frac{1}{2}\rho(U_t \cos\psi)^2 C_{LP} A_t \sin\gamma\cos\gamma \\ &\quad + \frac{1}{2}\rho C_{LV}(U_t \cos\psi)^2 (\sin^2\gamma)\cos\gamma A_t \\ D^{tail} &= \frac{1}{2}\rho(U_t \cos\psi)^2 C_{LP} A_t (\sin^2\gamma)\cos\gamma \\ &\quad + \frac{1}{2}\rho C_{LV}(U_t \cos\psi)^2 (\sin^3\gamma)\cos\gamma A_t \end{aligned} \tag{11}$$

In order to verify equation (9), a flapping wing robot was tested in a wind tunnel and the results of tail force were compared with the results of equation (9). The robot is shown in Figure 8. The comparison of the forces obtained from equation (9) with the forces measured in the wind tunnel test is shown in Figure 9. As shown in Figure 9, in order to obtain pure force exerted on the tail, the force created on a complete robot has been deducted from the force created on a tailless one.

The lift and drag forces obtained from equation (9) are in good agreement with test results because of the considerations of leading edge vortex.

Control design

The mathematical model of the robot can be expressed as the following

$$\dot{\chi} = f(\chi) + h(\chi, \boldsymbol{u}) \tag{12}$$

where f and h are nonlinear functions, $\chi = [\, x \;\; y \;\; z \;\; \dot{x} \;\; \dot{y} \;\; \dot{z} \;\; \theta_x \;\; \theta_y \;\; \theta_z \;\; w_1 \;\; w_2 \;\; w_3 \,]^T$ is the vector of state variables and

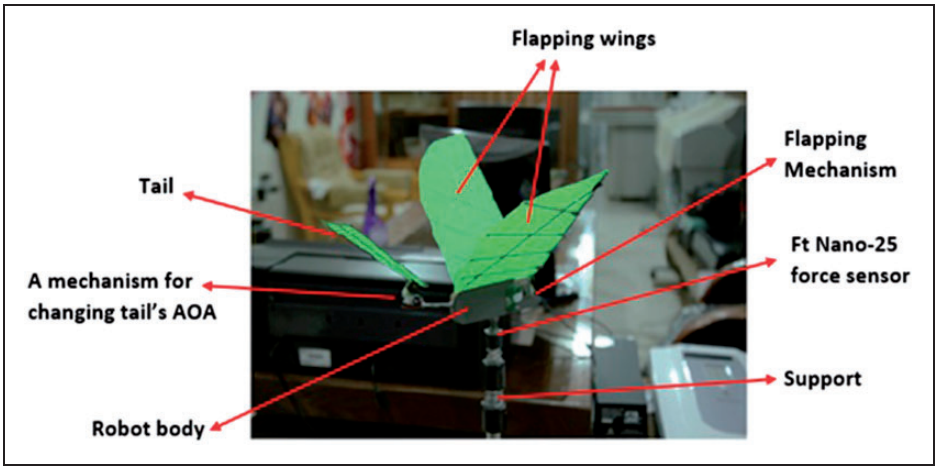

Figure 8. Flapping robot used in wind tunnel test.

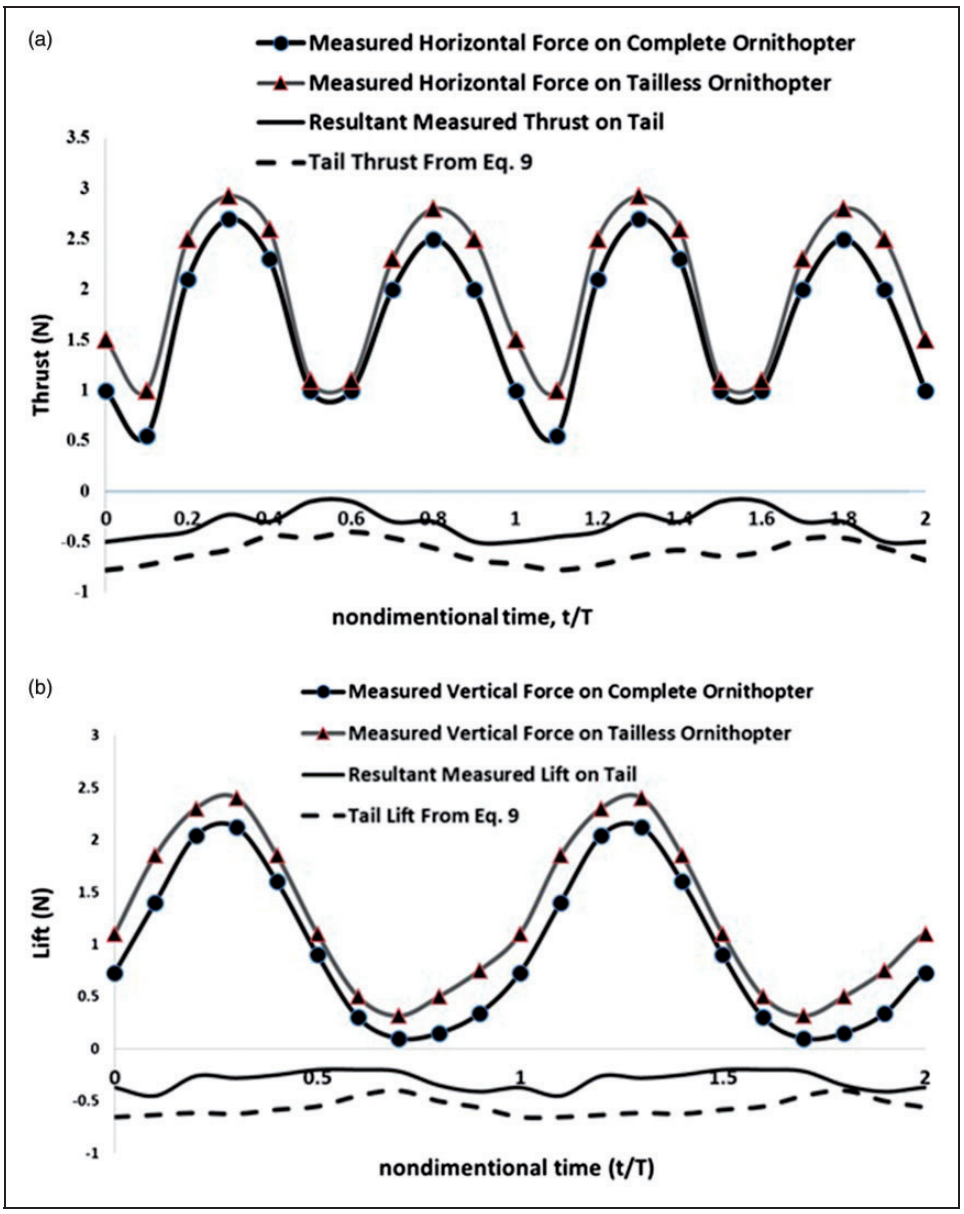

Figure 9. Comparison between tail force calculated from equation (9) and force measured in wind tunnel test for flapping frequency of 5 Hz, $U_\infty = 5\,\text{m/s}$, $\varphi_b = 0^\circ$, and $\beta_0 = 35^\circ$. (a) Thrust force; (b) lift force.

$\boldsymbol{u} = \begin{bmatrix} \theta_0 & \alpha_0 & \nu & \psi & \gamma \end{bmatrix}^T$ is the vector of input variable. All five input variables can be used to control the robot.

The purpose of the control system is to determine the input $\boldsymbol{u}$ so that the state vector reaches a desirable x_{ref} value. For this, the system error vector is defined in equation (13)

$$\boldsymbol{e} = \chi - \chi_{ref} \tag{13}$$

To assure the convergence of the method, the input u is assumed to meet equation (14)

$$f(\chi) + h(\chi, \boldsymbol{u}) - \dot{\chi}_{ref} = -\lambda \boldsymbol{e} \tag{14}$$

where λ is a constant and positive value. Then one can find the input of control system, $\boldsymbol{u}$, by solving equation (14) using the Newton–Raphson method, as follows

$$\begin{aligned} \boldsymbol{u}_{k+1} &= \boldsymbol{u}_k - \left(J_k'.J_k\right)^{-1}.J_k' \\ &\quad .\left[f(\chi_k) + h(\chi_k, u_k) - \dot{\chi}_{ref} + \lambda e_k\right] \\ \boldsymbol{e}_k &= \chi_k - \chi_{ref} \end{aligned} \tag{15}$$

where J_k is the Jacobian matrix

$$J_k = \left.\frac{\partial h(\chi, u)}{\partial u}\right|_{\chi=\chi_k,\ u=u_k} \tag{16}$$

And $\boldsymbol{e}_k$ is the error at the kth iteration

$$\boldsymbol{e}_k = \chi_k - \chi_{ref} \tag{17}$$

The limit of iterations is determined by the following inequality

$$\left|\boldsymbol{u}_{k+1} - \boldsymbol{u}_k\right| < \varepsilon \tag{18}$$

In other words, the appropriate input vector satisfies the above inequality.

Simulation results

In this section, the performance of the designed controller is verified by controlling the robot to track the curve c: $P_1(\mathrm{x}) = P_1(\mathrm{x}) = 0$. Also, $\mathrm{x} = [x \quad y \quad z]^T$ is the position vector of robot in the space. The desired path is $x^2 + (z-100)^2 - 10000 = \ y - 15 = 0$ which is a circle in horizontal plane. In this case, χ_{ref} and the initial variables are as follows

$$\begin{aligned} \mathrm{x}_0 &= \begin{bmatrix} 0 & 15 & 200 \end{bmatrix}^T \\ u_0 &= \begin{bmatrix} \frac{\pi}{4}\,(rad) & \frac{\pi}{12}\,(rad) & 5\,(Hz) & 0\,(rad) & 0\,(rad) \end{bmatrix}^T \\ \chi_{ref} &= \begin{bmatrix} x & 15 & \sqrt{10000 - x^2} + 100 \end{bmatrix}^T \end{aligned} \tag{19}$$

Also, the design parameters of the ornithopter are presented in Table 1. Simulating the model shows the acceptable coverage of the path by the robot as presented in Figure 10.

Table 1. Design parameters of the ornithopter.

Total mass (g)	42
Wing length (mm)	350
Wing area (mm^2)	52,000
Wing mass (g)	8
Tail chord (mm)	110
Tail area (mm^2)	5610
Flapping frequency (Hz)	1–7
flapping angle amplitude, β_0 (deg)	50

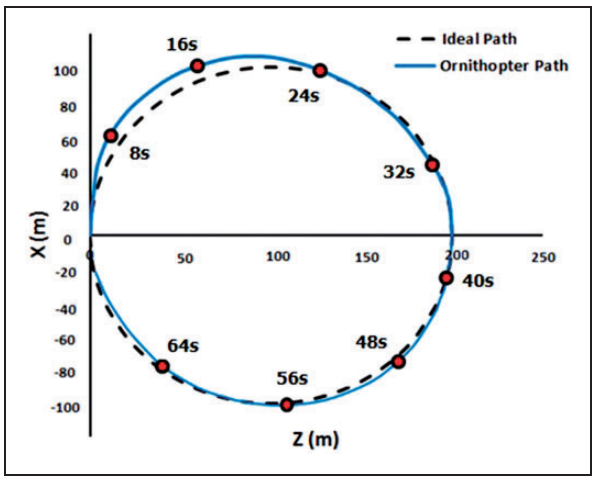

Figure 10. Actual and reference paths.

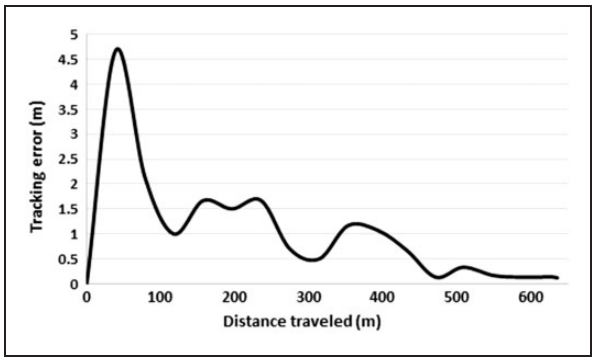

Figure 11. Tracking error of the robot.

As shown in Figure 10, at the beginning of the movement, the difference between the traveled and ideal path is greater than elsewhere. Because the control system requires time to reduce the amount of error and converge to the ideal path. The tracking error can be expressed as

$$\begin{aligned} E(t) = \sqrt{(x(t) - 100sin(0.204t))^2 + (y(t) - 15)^2} \\ + (z(\tau) - 100cos(0.204\tau) - 100)^2 \end{aligned} \tag{20}$$

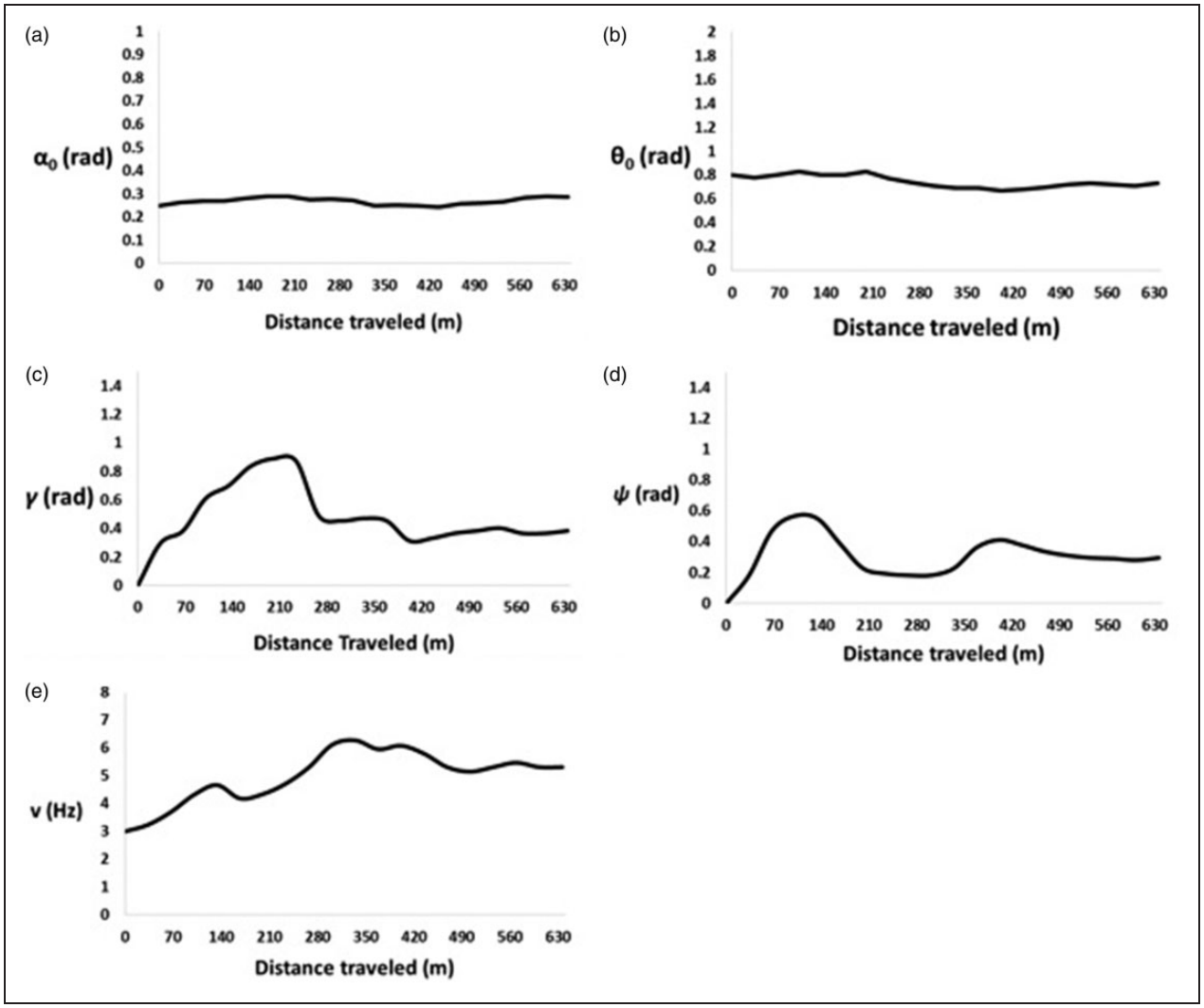

Figure 12. The control inputs along traveled path. (a) AOA of root; (b) flapping amplitude; (c) tail pitch angle; (d) tail roll angle; (e) flapping frequency.

The tracking error of the robot is shown in Figure 11. As shown in Figure 11, the error is high at the beginning of simulation and decreases as the robot travels the path. It is indicated that the designed controller is feasible and acceptable.

The changes of the five control inputs along the traveled path are presented in Figure 12. It is observed in Figure 12 that although the tail angles (ψ *and* γ) and wings flapping frequency (v) vary along the path, the amplitude of AOA (α_0) and amplitude of flapping (θ_0) do not change considerably.

Conclusion

In this paper, the dynamic and control models of a flapping wing robot are investigated. In the first section, a complete dynamic model for tail and wings is developed, and some experiments are performed to verify the analytical model of the tail. In the second section, a controller, based on NDI method, is designed to control the robot. The main conclusions of the study are given as follows:

1. There are good correlations between predicted values and *experimental results of tail forces at low and high angles of attack*. *This* reveals that the total force exerted on tail is caused by pressure difference on tail surfaces and also by leading edge vortices. The force exerted on tail at any position can be calculated using equations obtained in this work.
2. The simulation results also show that desired path can be successfully tracked by the robot and the tracking error converges to zero. This exhibits the performance of the NDI controller in flapping wing robots.
3. Numerical simulations of the control system show that the roll and pitch angles of the tail change remarkably along the path and the tail can be used as a control tool in guiding the robot along a curved path and in creating out of

plane motions. The tail can also enhance stability and maneuverability of the robot as in real birds.

Declaration of Conflicting Interests

The author(s) declared no potential conflicts of interest with respect to the research, authorship, and/or publication of this article.

Funding

The author(s) received no financial support for the research, authorship, and/or publication of this article.

References

1. Jones RT. The unsteady lift of a wing of finite aspect ratio. NACA Report No. 681. VA, USA: Langley Aeronautical Lab, 1940.
2. Ellington CP. The aerodynamics of hovering insect flight, III. Kinematics. *Phil Trans R Soc B* 1984; 305: 41–78.
3. DeLaurier JD. An aerodynamic model for flapping wing flight. *Aeronaut J R Aeronaut Soc* 1993; 97: 125–130.
4. Rahnejat H. *Multi-body dynamics: vehicles, machines and mechanisms*. Warrendale, PA: Society of Automotive Engineers, 1998.
5. Yuan X and Zhu J. Inverse dynamic modeling and analysis of a coaxial helicopter's swashplate mechanism. *Mech Mach Theory* 2017; 113: 208–230.
6. Ansari SA, Zbikowski R and Knowles K. Aerodynamic modelling of insect-like flapping flight for micro air vehicles. *Progr Aerosp Sci* 2006; 42: 129–172.
7. Zakaria MY, Elshabka AM, Bayoumy AM and Abdelhamid OE. Numerical aerodynamic characteristics of flapping wings. In: *13th International Conference on Aerospace Sciences & Aviation Technology*; ASAT-13, Cairo, Egypt, 26–28 May 2009.
8. Djojodihardjo H, Ramli AS and Wiriadidjaja S. Kinematic and aerodynamic modelling of flapping wing ornithopter. *Procedia Eng* 2012; 50: 848–863.
9. Shyy W, Aono H, Chimakurthi SK, et al. Recent progress in flapping wing aerodynamics and aeroelasticity. *Progr Aerosp Sci* 2010; 46: 284–327.
10. Lee JS, Kim JK, Han JH, et al. Periodic tail motion linked to wing motion affects the longitudinal stability of ornithopter flight. *J Bionic Eng* 2012; 9: 18–28.
11. Thomas ALR. On the aerodynamics of bird tails. *Phil Trans R Soc Lond* 1993; 50: 361–380.
12. Schenato L, Campolo D and Sastry SS. Controllability issues in flapping flight for biomimetic MAVs. In: *IEEE conference on decision and control,* Maui, Hawaii, 9–12 December 2003, vol. 6, pp.6441–6447. IEEE.
13. Deng X, Schenato L and Sastry S. Flapping flight for biomimetic robot insects: part II – flight control design. *IEEE Trans Robot* 2006; 4: 789–803.
14. Doman DB, Oppenheimer MW and Bolender MA. Altitude control of a single degree of freedom flapping wing micro air vehicle. In: *AIAA guidance, navigation and control conference*, Chicago, IL, 10–13 August 2009, AIAA-2009-6159.
15. Duan H, LI Z and LI Q. Model and control of micro flapping-wing aerial robot. In: *2010 international conference on computer design and applications*, Qinhuangdao, China, 25–27 June 2010, 3, pp.8–12.
16. Leong CW, Viet NQ and Debiasi M. Pitch and yaw control of tailless flapping wing MAVs by implementing wing root angle deflection. In: *International micro air vehicle conference and competition* 2014, pp.34–41. Delft, Netherlands: Delft University of Technology.
17. Ladopoulos EG. Non-linear singular integral representation for unsteady inviscid flowfields of 2-D airfoils. *Mech Res Commun* 1995; 1: 25–34.
18. Xia X and Mohseni K. Lift evaluation of a two-dimensional pitching flat plate. *Phys Fluid* 2013; 25: 091–109.
19. Nikos J and Domingo A. *The aerodynamics of delta wings of with separated flow elliptical cross-section*. Stanford, CA: Stanford University, 1985.
20. Polhamus EG. *A concept of the vortex lift of sharp edge delta wings based on a leading edge suction analogy*. NASA TN-D-376. Washington DC, USA: NASA, 1966.

Appendix

Notation

A_t	tail area
C	section chord
C_D	drag coefficient
C_L	lift coefficient
C_{LP}	lift coefficient due to pressure difference on the tail surfaces
C_{LV}	lift coefficient due to leading edge vortices
D	drag
E	tracking error
f	vector of forces
F	potential function
I	moment of inertia of the body
L	lift
m	robot mass
N	force normal to the wings chord
T	thrust
$\boldsymbol{u}$	control vector
U_∞	freestream velocity
U_{rel}	relative velocity of wind
v^b	velocity vector in body frame
w	vector of angular velocity
α	relative angle of attack
β	flapping angle
γ	pitch angle of tail
θ	body angle
ν	flapping frequency
τ	vector of moments
χ	state vector
φ_b	angle of flapping axis with respect to U_∞
φ_w	angle of chord with respect to flapping axis
$\delta\varphi$	angle of wing twisting
ψ	roll angle of tail